Tellus SERIES A DYNAMIC METEOROLOGY AND OCEANOGRAPHY
PUBLISHED BY THE INTERNATIONAL METEOROLOGICAL INSTITUTE IN STOCKHOLM

Tellus (2009)

TELLUS

# Observation of polar lows by the Advanced Microwave Sounding Unit: potential and limitations

*By* C. CLAUD[1]*, B. M. FUNATSU[1], G. NOER[2] and J.-P. CHABOUREAU[3], [1]*Laboratoire de Météorologie Dynamique/IPSL, CNRS, Ecole Polytechnique, 91128 Palaiseau, France;* [2]*The Norwegian Meteorological Institute, Forecasting Division of Northern Norway, Tromsoe, Norway;* [3]*Laboratoire d'Aérologie, University of Toulouse and CNRS, Toulouse, France*

(Manuscript received 9 June 2008; in final form 20 November 2008)

ABSTRACT

The potential of the Advanced Microwave Sounding Unit (AMSU) observations for the depiction and tracking of intense high-latitude mesoscale maritime weather systems, called polar lows, is explored. Since a variety of mechanisms are important for their development and maintenance, this investigation is based on three polar low cases of different types. The AMSU-B channels at 183 GHz are able to locate convective polar lows (PL) even in their incipient stage, at a time when there is considerable uncertainty as to the nature of the cloud structures seen in the visible or infrared imagery. This detection is based on temperature depression due to scattering by hydrometeors, as confirmed by comparison with radar data. These same channels will, however, fail to unambiguously detect weakly convective and mainly baroclinic PL. The AMSU-A channels help documenting the large-scale environment in which PL develop. Channel 5 clearly shows the cold air outbreaks associated with these developments, whereas the difference between channels 7 and 5 can be used to detect and locate positive upper-level potential vorticity anomalies. Because of the high temporal availability of AMSU observations and despite some limitations pointed out in this study, these results are relevant for PL forecasting and monitoring.

## 1. Introduction

Polar lows (PL) are intense mesoscale maritime weather systems, which form during wintertime over high-latitude regions. Over the North Atlantic, they are commonly observed over the Norwegian, Barents, Kara (e.g. Rasmussen and Turner, 2003) and Labrador Seas (Rasmussen et al., 1996). They occur during cold air outbreaks and are generally associated with heavy snowfalls and surface winds which can be in excess of 30 m $s^{-1}$. However, they still represent a challenge in terms of forecasting: their small scale extent (100–1000 km) and short lifetime (average 15–20 h; Wilhelmsen, 1985), the absence or rarity of synoptic observations and real-time satellite derived winds, the poor radar coverage and, in many cases, unreliable model fields lead to a rather low skill, and some PL even go undetected until they affect coastal regions.

For years, it has been difficult to formulate a brief, unambiguous polar low defintion, partly because a variety of mechanisms can play a role and be important for the development and maintenance of these systems. A long controversy existed on whether baroclinic instability (e.g. Harrold and Browning, 1969; Mansfield, 1974; Duncan, 1977; Nordeng and Rasmussen, 1992), conditional instability of the second kind (CISK) or wind-induced surface heat exchange (WISHE) in which the primary energy source is fluxes of heat from the ocean to the atmosphere, the role of convection being to transport the energy through the troposphere (e.g. Emanuel, 1986; Emanuel and Rotunno, 1989; Rasmussen, 1989), would better expain such developments. It was finally agreed that PL appear in many forms, leading to the idea of a 'spectrum' of mesoscyclones (Turner et al., 1993) going from purely baroclinic to purely convective sytems, including hybrid systems. There is now a consensus on the following definition (Heinemann and Claud, 1997), used throughout this paper: the term polar mesocyclones is the generic term for all meso-a and meso-b cyclonic vortices poleward of the main polar front (scale definition according to Orlanski, 1975). The term polar low should be used for intense maritime polar mesoscale cyclones with scales up to 1000 km with a near-surface wind speed exceeding 15 m $s^{-1}$. Depending on the nature of the mechanisms at play, cloud fields show certain basic, characteristic signatures, but in general the visual impression in infrared/visible imagery of PL is similar to the better known tropical cyclones, with cloud bands and an eye at the centre, though their extent and intensity are smaller.

Because of the lack of in situ observations over the development areas, satellite data offer the best way to observe these

*Corresponding author.
e-mail: chclaud@lmd.polytechnique.fr
DOI: 10.1111/j.1600-0870.2008.00384.x

storms. Information from polar-orbiting satellites have indeed been used during the last two decades to document PL environment and structure (e.g. Claud et al., 1992a,b, 1993, 2004; Turner et al., 1992). These studies have shown that the most comprehensive view of PL is provided by the synergetic use of multiple instruments; it increases the amount and kind of variables and also the temporal resolution, which over these areas is already good due to the overlapping of successive passes (e.g. Claud et al., 1993; Carleton et al., 1995; Heinemann, 1996; Moore et al., 1996; Lieder and Heinemann, 1999).

Among the variety of instruments and therefore wavelengths that can be used for PL observations, the potential of microwave wavelengths has been largely demonstrated in the past. The Scanning Multichannel Microwave Radiometer (SMMR) sensor, with channels at 19 and 37 GHz (Gloersen et al., 1989; Rasmussen et al., 1992), and then the Special Sensor Microwave Imager (SSM/I), with additional frequencies at 22 and 85 GHz, have been extensively used (e.g. McMurdie et al., 1997; Hewson et al., 2000; Claud et al., 2004). Their advantage over infrared (IR) measurements is that they penetrate clouds and are sensitive to those characterized by large ice particles. This property can precisely be used to detect and track PL through the presence of convective cells as shown by Claud et al. (1992a) using 85 GHz measurements on SSM/I. The launch of the Advanced Microwave Sounding Unit (AMSU) instrument package first in 1998 on NOAA-15, with an increased number of frequencies including 89 and 183 GHz and an improved spatial resolution up to 16 km, should increase the knowledge on PL characteristics and environment. However, so far, to the knowledge of the authors, AMSU data have been used only once for the study of a PL (Moore and Vonder Haar, 2003). These authors showed how the warm core structure of a PL that occurred in the Labrador Sea on 17–18 March 2000 could be identified by AMSU measurements at 53.6 GHz (AMSU-A channel 5). They also suggested that observations at 50, 89 and $183 \pm 3$ GHz could provide additional insight into the PL structure and environment in terms of cloudiness, surface variability and moisture, though the analysis of these last frequencies was undertaken solely in an attempt to better characterize the structures at 53.6 GHz. In this study, we propose an extension of the work of Moore and Vonder Haar (2003), showing how high frequencies offer new possibilities of early detection and tracking of PL. In addition, a description of the synoptic environment can also be inferred from channels sounding around 55 GHz. Since PL appear in many forms, the exploration of the potential of AMSU observations is based on three case studies that have been chosen to cover the wide spectrum of PL. This will also allow to show some limitations of AMSU regarding its ability to detect some types of PL.

The paper is organized as follow. In Section 2, a description of AMSU data and the necessary pre-processing are presented. In Section 3, a brief synoptic analysis of the three case studies is given. AMSU observations of PL developments are presented in the following section. Finally, the results from the analysis are summarized and discussed in Section 5. Advantages as well as limitations that can be expected from the use of AMSU for PL research and forecasting are highlighted.

## 2. The AMSU data

The AMSU instrument has been collecting observations onboard of NOAA-15, 16, 17 and 18 polar-orbiting satellites starting in 1998, 2000, 2002 and 2005, respectively. AMSU, whose swath width is of approximately 2300 km, consists of two modules—AMSU-A and AMSU-B. AMSU-A, with 12 of 15 channels between 50 and 58 GHz in the Oxygen band (Table 1), allows the observation of the temperature structure of

*Table 1.* Frequencies and bandwidth of AMSU-A and B channels

| AMSU-A | | | AMSU-B | | |
|---|---|---|---|---|---|
| Channel number | Centre freq. (GHz) | Bandwidth (MHz) | Channel number | Centre freq. (GHz) | Bandwidth (MHz) |
| 1 | 23.80 | 251 | 1 | 89 | 5000 |
| 2 | 31.40 | 161 | 2 | 150 | 4000 |
| 3 | 5.30 | 161 | 3 | $183 \pm 1$ | 1000 |
| 4 | 52.80 | 380 | 4 | $183 \pm 3$ | 2000 |
| 5 | $53.59 \pm 0.115$ | 168 | 5 | $183 \pm 7$ | 4000 |
| 6 | 54.4 | 380 | | | |
| 7 | 54.94 | 380 | | | |
| 8 | 55.50 | 310 | | | |
| 9 | 57.29 ($f_0$) | 310 | | | |
| 10 | $f_0 \pm 0.217$ | 76 | | | |
| 11 | $f_0 \pm 0.320 \pm 0.048$ | 34 | | | |
| 12 | $f_0 \pm 0.322 \pm 0.022$ | 15 | | | |
| 13 | $f_0 \pm 0.322 \pm 0.010$ | 8 | | | |
| 14 | $f_0 \pm 0.322 \pm 0.004$ | 3 | | | |
| 15 | 89.00 | 2000 | | | |

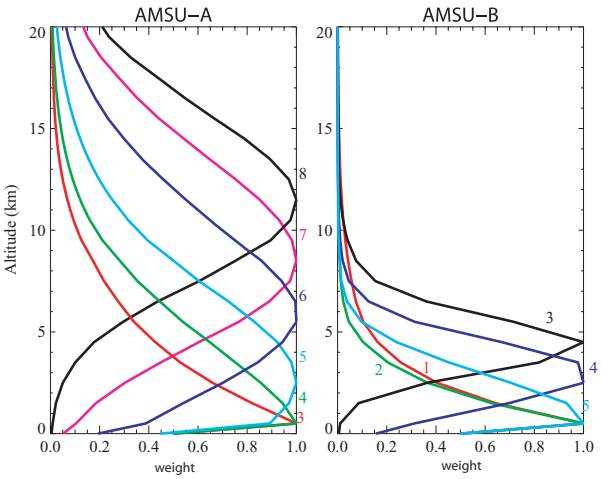


*Fig. 1.* Normalized weighting functions for the AMSU-A temperature channels sounding in the troposphere (3–8) and AMSU-B channels at nadir, for a subarctic profile.

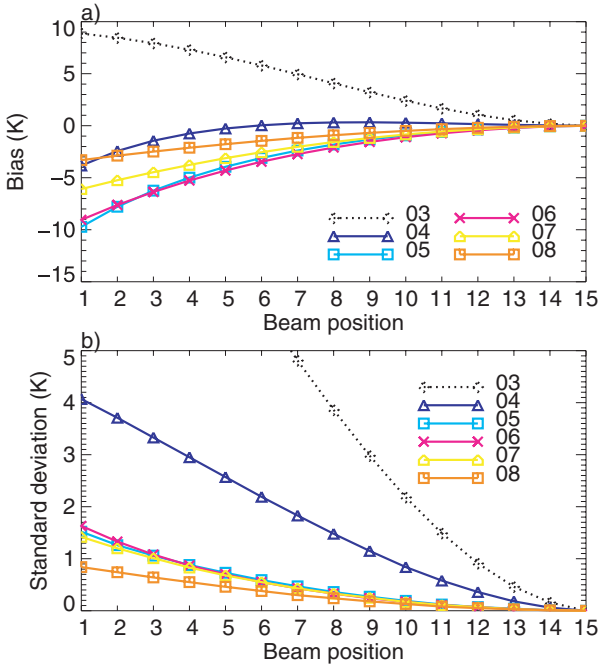


*Fig. 2.* RTTOV derived brightness temperatures average bias (a) relative to the nadir position and associated standard deviation (b) for tropospheric channels for AMSU-A as a function of angle of view. Only the first half number of beams is shown.

the atmosphere from the surface until 40 km (Fig. 1). Its spatial resolution ranges from 48 km at nadir to about 150 km at the edges of the swath. AMSU-B has two atmospheric window channels (at 89 and 150 GHz) and three channels along the wings of the $H_2O$ absorption band centred at 183 GHz (Table 1). These three channels provide data on the atmospheric humidity on the upper (B-3), middle (B-4) and lower (B-5) troposphere whereas channels B-1 and B-2 enable deeper penetration through the atmosphere to the surface (Fig. 1). At the frequencies of AMSU-B, clouds are almost transparent whereas rain and snow are strong scatterers, so that this instrument can also be used to map precipitation. The spatial resolution of AMSU-B is of 16 km nadir and 52 km at the edges.

Early NOAA-15 observations suffered from antenna interference problems during the period 1998–1999 (Mo, 1999). This problem has been corrected subsequently; however, scan asymmetries with respect to the angle of view in NOAA-15 AMSU-B can be large (Buehler et al., 2005), and therefore we have favoured, whenever possible, the use of data from NOAA-16 and 17 in this study. For NOAA-15 passes that have nevertheless been used, we have checked that the asymmetry was minor.

AMSU-A brightness temperatures (BT) must be corrected for the zenith angle affect due to the fact that a thicker layer of the atmosphere is probed as the field of view departs from the nadir position. This leads to colder temperatures at the edge of the orbits for channels sounding the troposphere. Several methods have been proposed to correct this effect (e.g. Wark, 1993; Goldberg et al., 2001), and they have been shown to reduce the effect to the noise level accuracy. In this study, AMSU-A BT have been adjusted using coefficients derived from the radiative transfer model Radiative Transfer for Tiros Operational Vertical Sounder (RTTOV) version 8.5 (Saunders et al., 2005), which is able to simulate realistically the AMSU BT (Bauer et al., 2006).

Figure 2a shows the RTTOV simulated BT biases between the angle of view and nadir for AMSU-A tropospheric channels, for three arbitrarily chosen days (one for each case study) and the North Atlantic area, whereas Fig. 2b shows the associated standard deviation. The biases for the channels that are not significantly affected by the surface, that is, channels 5, 6 and 7, are −11, −10 and −6.5 K, repectively, whereas the standard deviation is of the order of 1.5 K. Lowermost tropospheric channels (3 and 4) present larger variability than upper tropospheric channels. The bias of simulated BTs relative to nadir is time-dependent (Fig. 3, top row for channels 5, 7 and 8) and latitude-dependent (Fig. 3, bottom row), with the bias decreasing with increasing latitude. Therefore a time- and latitude-dependent set of coefficients is applied to correct BT for the limb effect. One further question is whether the influence of the surface in the BT for these three channels would yield different sets of coefficients for land and ocean. The difference in bias being less than 1 K (not shown), even for large viewing angles, a single (time- and latitude-dependent) set for both sea and land was chosen. For module B, only Greenwald and Christopher (2002) reported a depression of up to 5 K due to limb effect in NOAA-15 AMSU-B channel 3, but since no further documentation of limb effect or its correction for AMSU-B was found, the data were used without applying any correction.

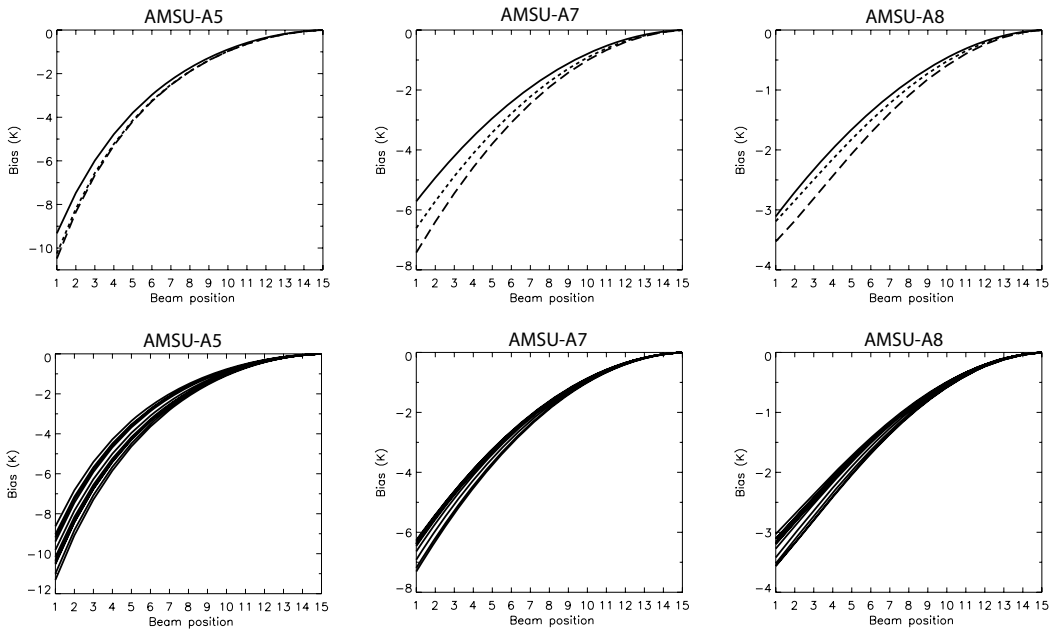


*Fig. 3.* RTTOV-derived limb-correction coefficients as a function of beam position (15 representing the near-nadir field of view), for channels shown on the top of each panel. Top row: different dates (solid, 00 UTC 17 December 2004; dotted, 00 UTC 20 January 2005; dashed, 00 UTC 06 March 2005); bottom row: different latitudes (average of three dates of top row, from 50 to 80°N every 2.5°).

## 3. Case studies

To fully explore the potential and limitations of AMSU for polar low observation, three very different cases—from mainly convective to mainly baroclinic at least in the incipient stage—have been chosen. In this section, a brief synoptic description of these three cases is given.

### *3.1. 18 December 2004*

The 17–18 December period was characterized by an outbreak carrying cold air from snow and ice covered areas over the Norwegian Sea. Early on 18 December, the northerly flow associated with the cold air outbreak was a result of a decaying synoptic low between Norway and Spitzbergen and a high over Greenland. The polar low formed in the early hours of the day, beginning as a cluster of Cumulo-Nimbus (Fig. 4a). At 18 UTC (Fig. 4b), it hit just south of the Lofoten Islands and was observed by a radar located over this area. Based on High Resolution Limited Area Model (HIRLAM) -10 km results, temperatures as low as −42 °C were prognosed at 500 hPa upstream of the low, but no closed circulation appeared on the 18-h-forecast. This convective polar low is typical of the majority of PL and corresponds to what used to be called primary (or real) PL (Rasmussen et al., 1993).

### *3.2. 21 January 2005*

This low lasted only from 12 to 21 UTC and reached Denmark. It was on the southern tip of a long north-south oriented deep surface trough with convection up to about 9 km. It was associated with a shallow upper trough and cold core, with the temperatures at 500 hPa being around −39 °C. The sea surface temperature being of around 7 °C, the difference between the sea surface temperature and the temperature at 500 hPa was just above the 43 °C threshold currently used for defining PL at the Norwegian Meteorological Institute (Noer and Ovhed, 2003; Claud et al., 2007). The low yielded winds of 25 m $s^{-1}$ measured on a boat in the central North Sea and more than 20 m $s^{-1}$ over a wider area (Fig. 4c). Unlike the preceding case, it was a rather atypical polar low, though belonging to the developments that may appear during cold air outbreaks, and is an hybrid in the spectrum with both convection and baroclinicity important to its development.

### *3.3. 7 March 2005*

This polar low development took place along a boundary layer front between Svalbard and northern Norway (Fig. 4d). It lasted about 12 h, and the associated circulation was very shallow (less than 2 km; B. Bruemmer, personnal communication, 2005). It, however, gave high wind speeds during the early stages (more than 20 m $s^{-1}$ measured locally at Bear Island) and, as such, can be considered as a polar low though fairly weak. This case is representative of PL forming through baroclinic instability.

## 4. AMSU observations of PL

### *4.1. 18 December 2004*

The three satellite suite (NOAA 15–17) available at that time offers a global sampling nearly every 4 h, but at high latitudes, a

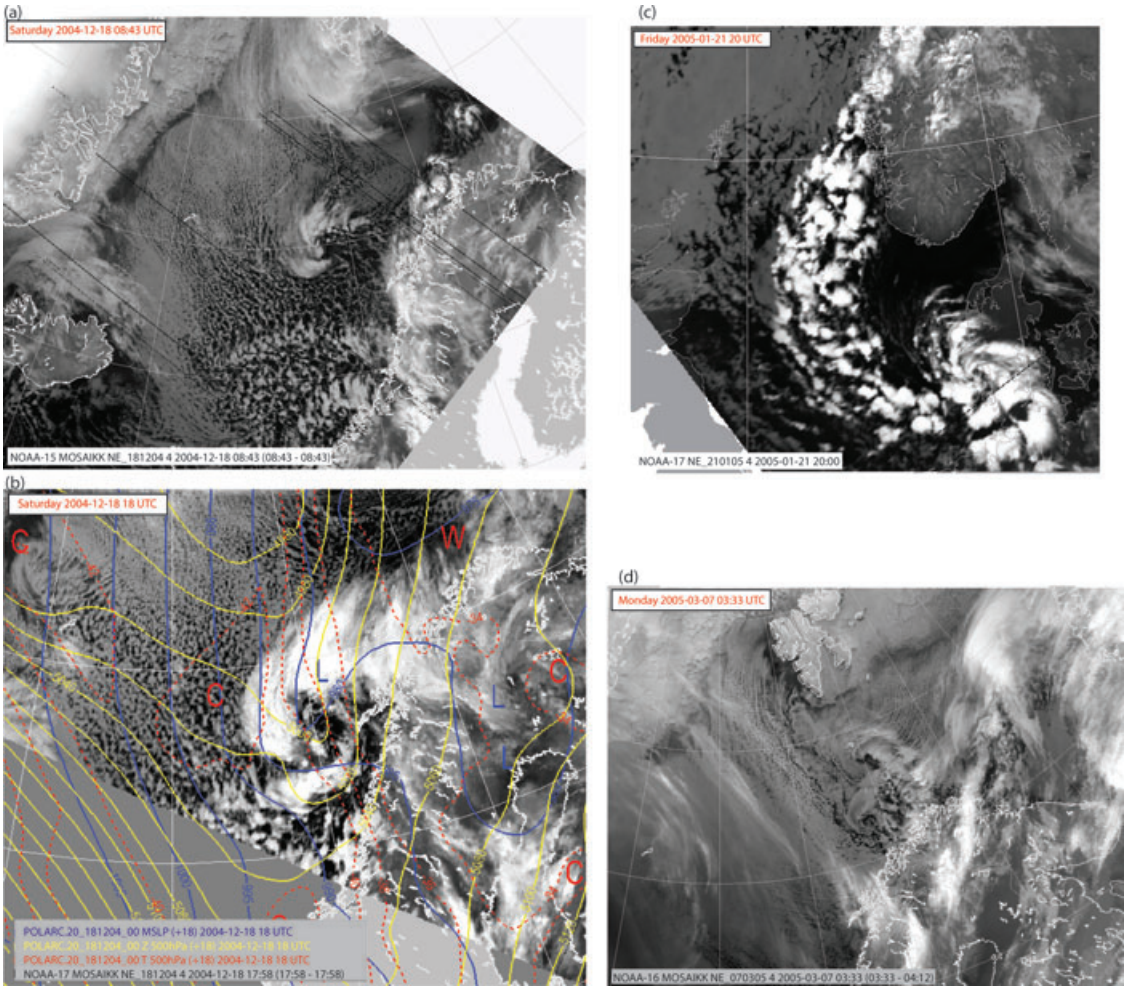


*Fig. 4.* Advanced Very High Resolution Radiometer (AVHRR) 11 $\mu$m imagery for (a) 18 December 2004, 08 UTC, NOAA-15; (b) 18 December 2004, 18UTC, NOAA-17; mean sea level pressure (mslp), as well as temperature and geopotential heights at 500 hPa (from HIRLAM-10 km, 18-h-forecast) have been superimposed; (c) 21 January 2005, 20 UTC, NOAA-17 and (d) 7 March 2005, 03 UTC, NOAA-16.

much more frequent sampling of any mesoscale system can be obtained due to overlapping swaths. Even if we exclude passes that only partially cover the polar low, we still have six good passes during the lifecycle of the disturbance.

For exploring the potential of AMSU-B channels for the monitoring of PL, and since this monitoring is based on the presence of large ice particles, we first present AMSU-B channels 2–5 for 18 UTC, 18 December 2004 (Fig. 5), that is, at a time when the polar low was within the radar range (Fig. 6). AMSU-B BTs show, in latitudes between 65°N and 70°N and longitudes between 5°E and 15°E, areas of colder temperatures due to scattering by hydrometeors corresponding to the PL, in fair agreement with higher reflectivity values in the radar image. For precipitating areas as depicted by the radar, channel 4 indicates values of the order of 240 K or below (and a BT depression of about 15 K compared with the environment), while values of about 234 K or below (and an approximate depression of about 20 K) are observed for channel 5. Using these thresholds, an early detection of the PL is possible, as shown on Figs. 7a and b displaying AMSU-B4 BT at 03 and 06 UTC, 18 December. At 03 UTC, convective areas are observed around 71°N 3°E and 72°N 5°E, and they move southeastwards subsenquently. This early detection has implications in terms of forecasting, since these systems develop in areas where in situ data are rare or even non-existent and outside of the radar coverage. At this time, there is considerable uncertainty as to the nature of the various cloud structures on visible and IR imagery. Even if the IR images at 03 and 06 UTC (not shown) suggest some cyclonic structure at the top of the clouds level, it is difficult to predict the potential for further development because the lowest layers are obscured by the cirrus shield. Channel 4 also permits the tracking of the PL during its whole lifecycle as can be seen on Fig. 7 showing the sequence from 03–20 UTC, 18 December. Similar results are obtained with channel 5 (not shown); channel 3 appears more noisy and shows less clearly the convective structures in their incipient stage, likely because it sounds higher in the

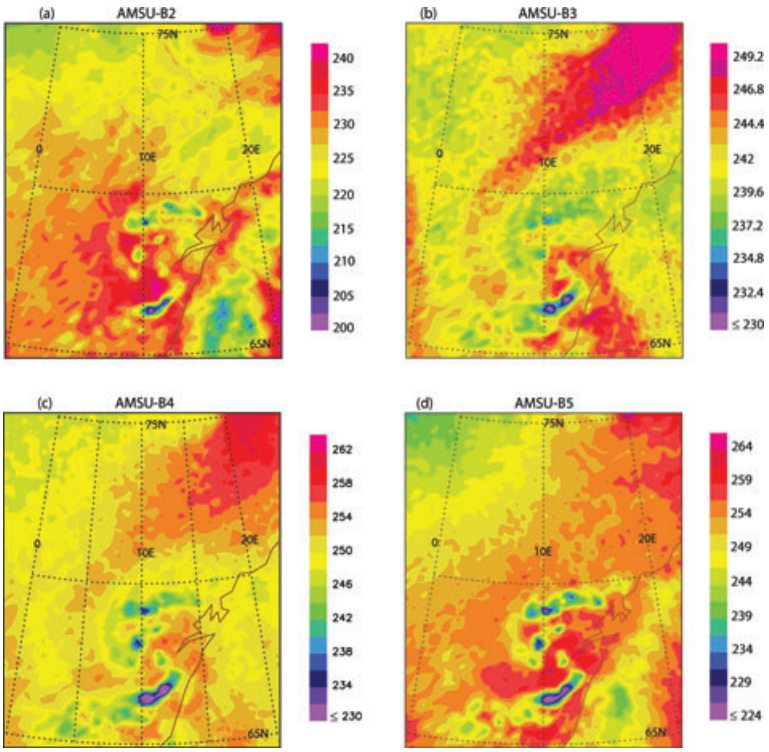


*Fig. 5.* NOAA-17 AMSU-B Brightness Temperature (in K) channel 2 to 4 for 18 UTC 18 December 2004.

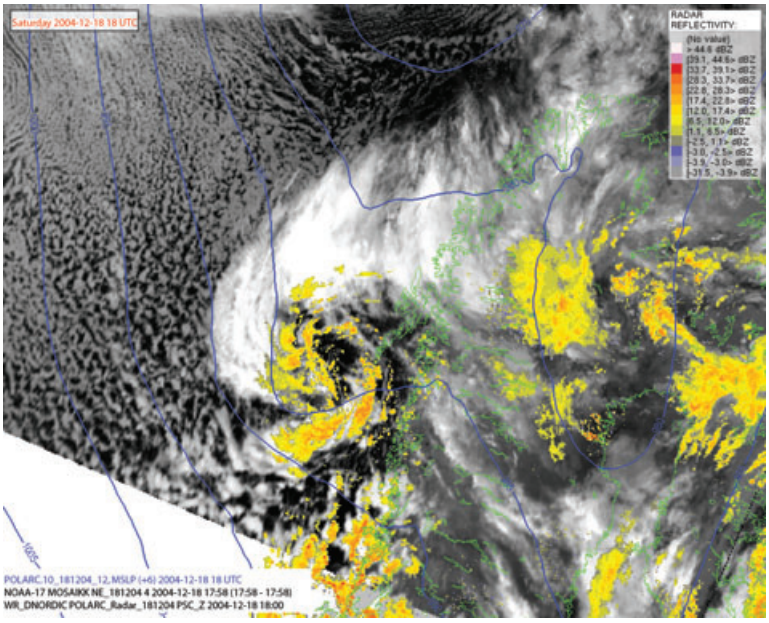


*Fig. 6.* Advanced Very High Resolution Radiometer (AVHRR) 11 $\mu$m imagery, mean sea level pressure (from HIRLAM-10 km, 6-h-forecast) and radar reflectivity for 18 UTC 18 December 2004.

atmosphere (Fig. 1) whereas PL are generally restricted to the first 5 km.

In addition, a synoptic description of the thermal environment in which the PL develop can be obtained from AMSU-A observations. The sequence of AMSU-A channel 5 from 03 UTC, 17 December, until 10 UTC, 18 December (Fig. 8), clearly shows the development of the cold air outbreak over the Norwegian Sea. At 12 UTC, 17 December (Fig. 8b), the gradient is very strong and tends to slacken a bit during the following hours.

As can be seen from Fig. 8, the spatial and vertical resolution of AMSU-A do not permit to infer precise thermal structures at the scale of the PL. This will be only very occasionnaly possible in the presence of a sufficiently large and deep signature, as it

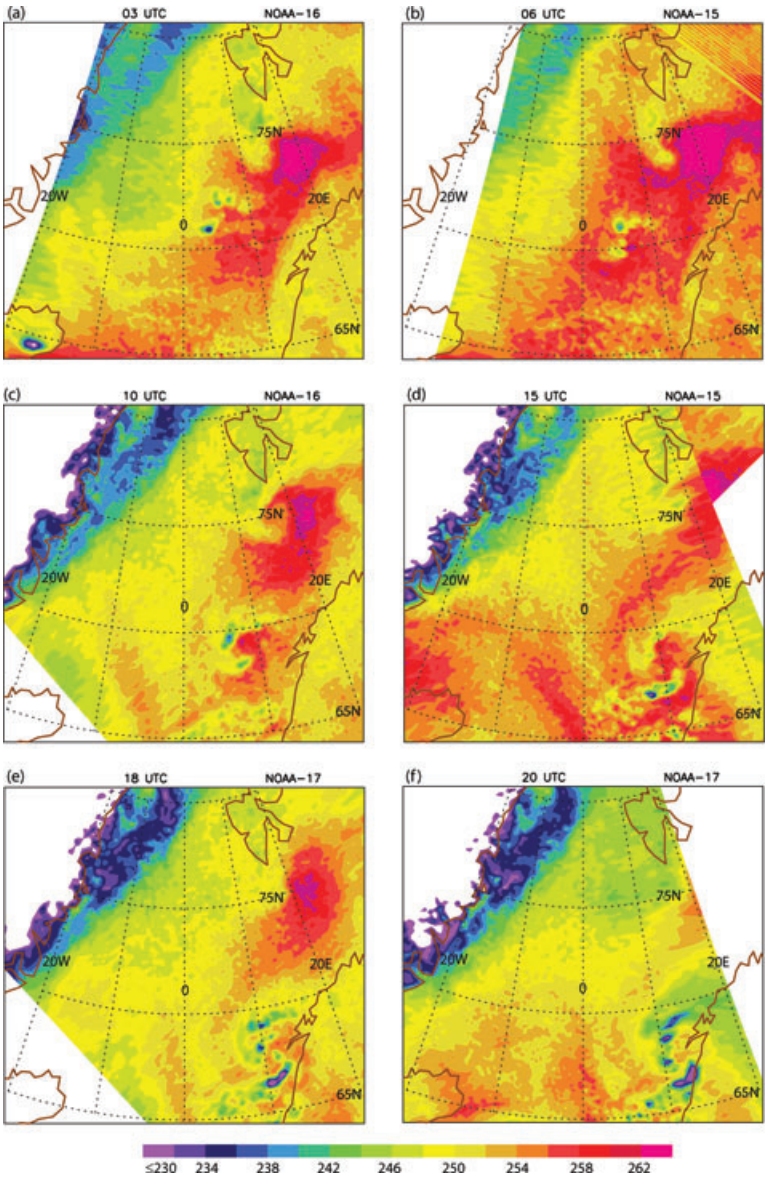


*Fig. 7.* AMSU-B channel 4 Brightness Temperature (in K) sequence for 18 December 2004: (a) NOAA 16, at 03UTC; (b) NOAA 15, at 06 UTC; (c) NOAA 16, at 10 UTC; (d) NOAA 15 at 15 UTC; (e) NOAA 17, at 18 UTC and (f) NOAA 17, at 20 UTC.

was the case for the PL studied by Moore and Von der Haar (2003).

### *4.2. 21 January 2005*

Like the preceding case, a very high sampling of this event is available, with six passes between 03 and 20 UTC. This case confirms the previous findings as can be seen on Fig. 9 showing AMSU-B4 and -B5 for passes at 11 and 20 UTC, respectively. The convective cells observed on IR imagery appear with AMSU-B4 and -B5 BT of the order or below 240 K. However, AMSU-B2 displays less sensitivity to the large ice particles, very likely due to its lower frequency and the position of the weighting function, well below the 9 km level corresponding to the upper level of convection. In addition, AMSU-B2 displays low values over other areas (around Iceland and along the eastern coast of Great Britain), and for these two reasons, it appears to be less efficient than channels 4 and 5 for the depiction of PL.

The AMSU-A5 also shows a very cold air outbreak that reached relatively southern latitudes (Fig. 10; 03 and 12 UTC, 21 January). The polar low developed shortly after the time when the gradient was the strongest.

Several PL have in common the presence of an upper-level positive potential vorticity (PV) anomaly, which, when passing over a region of low-level baroclinicity, triggers the development at the surface. Such a positive PV anomaly corresponds to an intrusion of stratospheric air into the troposphere. Because of the stratospheric origin and the downward vertical penetration,

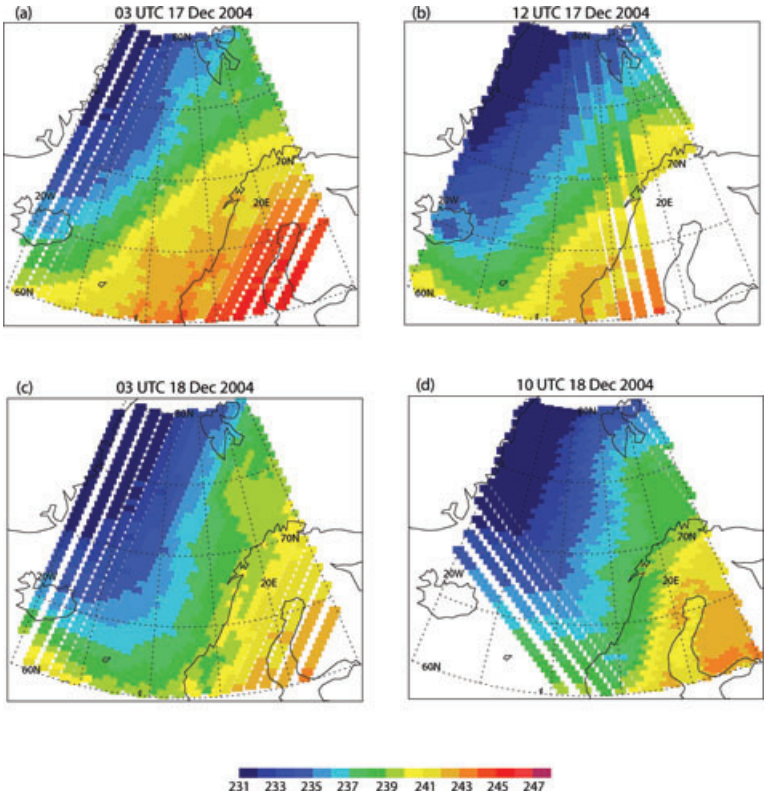


*Fig. 8.* Limb-corrected NOAA-16 AMSU-A channel 5 Brightness Temperature (in K) sequence for 17–18 December 2004: a) 03 UTC 17 December; (b) 12 UTC 17 December; (c) 03 UTC 18 December and (d) 10 UTC 18 December.

the associated thermal anomaly is positive (i.e. warm). In a recent study dedicated to AMSU observations of Mediterranean systems, Funatsu et al., (2007) demonstrated that AMSU-A8 BT was suitable for the detection of upper-level structures. In addition, the difference between AMSU-A channels 7 and 5, in which the lower troposphere part of the signal is removed from channel 7, could detect deep intrusions. We found that AMSU-A8 could not be used for the same purpose in high-latitude regions, because stratospheric intrusions are probably too shallow, the weighting function peaks too high (Fig. 1) and the sensitivity of the channel is not sufficient. However, of interest is the fact that the difference between AMSU-A channels 7 and 5 for the orbit at 03 UTC shows an area of increased difference (i.e. less negative) situated roughly between Denmark and Iceland, with a local maximum to the south of Norway (Fig. 11). This feature appears also on PV fields at 300 hPa from ECMWF (Fig. 12a) and on the vertical cross-section at 63°N (Fig. 12b), suggesting a possible PV interaction in the PL development. This feature was very likely associated with the presence of a synoptic low over this area some time before the development of the PL.

### *4.3. 7 March 2005*

Four passes at 03, 07, 09 and 11 UTC are available during the lifecycle of the PL. Looking at AMSU-B channels 2, 4 and 5 at 03 UTC (Figs. 13a, c and e), there is no clear indication of very low values due to scattering that could permit to detect and/or track the PL. Only a very small area with colder BT values appears in AMSU-B5 at 74°N 21°E and then at 11 UTC at a latitude of 71°N, between approximately 18°E and 27°E (Figs. 13b, d and f). These convective areas are seen in the eastern cloud structure forming the PL, whereas the western one appears as warmer than its environment due to its microphysical composition (the signal emitted by precipitation overcomes the scattered one). A close inspection of AMSU-B2 channel also indicates low BT values in the convective part of the clouds, which are, however, difficult to distinguish from their immediate environment. This case shows that for PL that are only marginally convective, a detection and tracking using the AMSU-B instrument will be ambiguous or even impossible.

However, as for the preceding cases, AMSU-A channel 5 (Fig. 14) shows a strong baroclinic area with very cold air (about 236 K) between Svalbard and Northern Norway and extending over the Barents Sea.

The difference between AMSU-A channels 7 and 5 for 7 March at 03 UTC is shown on Fig. 15. As for the 21 January PL, an area of reduced difference appears to the northeast of the orbit. This feature is in qualitative agreement with ECMWF PV fields in the upper troposphere (Figs. 12c and d) and indicates the presence of a strong PV anomaly that has very likely played an important role in the development of the polar low.

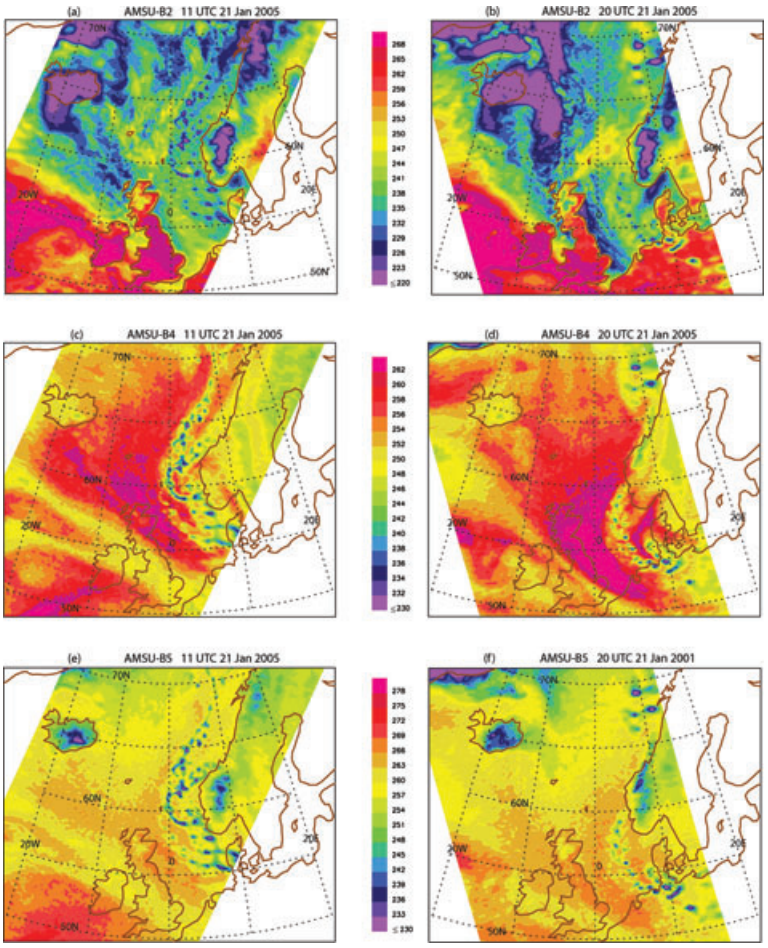


*Fig. 9.* NOAA-17 AMSU-B channels 2, 4, 5 Brightness Temperature (in K) for 21 January 2005 at 11 (a, c, e) and 20 UTC (b, d, f).

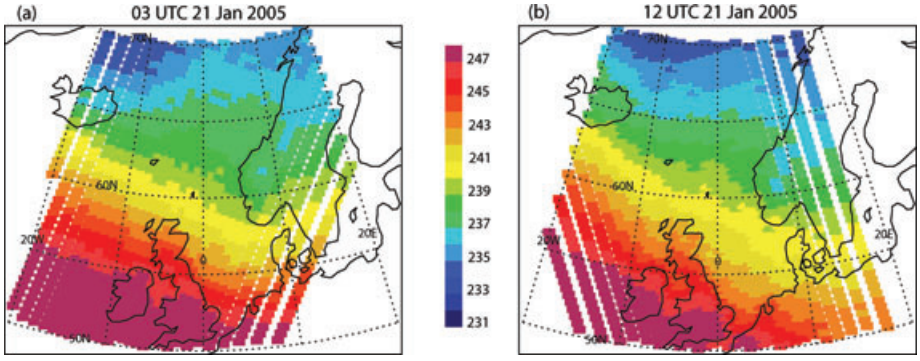


*Fig. 10.* Limb-corrected NOAA-16 AMSU-A channel 5 Brightness Temperature (in K) for 21 January 2005 at (a) 03 and (b) 12 UTC.

## 5. Discussion and summary

There has now been a number of studies aiming at showing the potential of the AMSU onboard the NOAA polar-orbiting satellites for tropical and mid-latitude storms (e.g. Kidder et al., 2000; Spencer and Braswell, 2001; Zhu et al., 2002; Brueske and Velden, 2003; Demuth et al., 2004; Funatsu et al., 2007, Yao et al., 2008). This study concentrates on polar oceanic regions where conventional observations are scarce and for which a single study has been conducted (Moore and Von der Haar, 2003). These regions are regularly affected by PL, which are characterized by severe weather that can take the form of strong and rapidly changing winds and dense snow showers. As a consequence, they often cause problems for the coastal fisheries, as well as interruptions for aviation and general traffic in the coastal areas. The AMSU has the advantage of having a finer vertical and horizontal resolution than previous vertical sounders (e.g. Heinemann et al., 1995), which makes it very attractive to

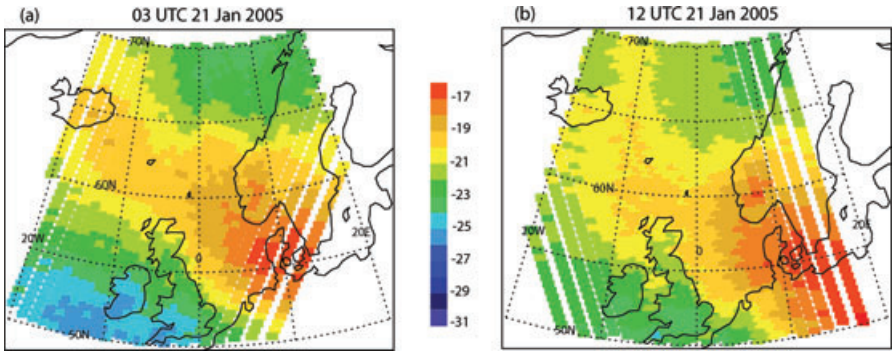


*Fig. 11.* Limb-corrected NOAA-16 AMSU-A channel 7 minus 5 Brightness Temperature (in K) for 21 January 2005 at (a) 03 and (b) 12 UTC.

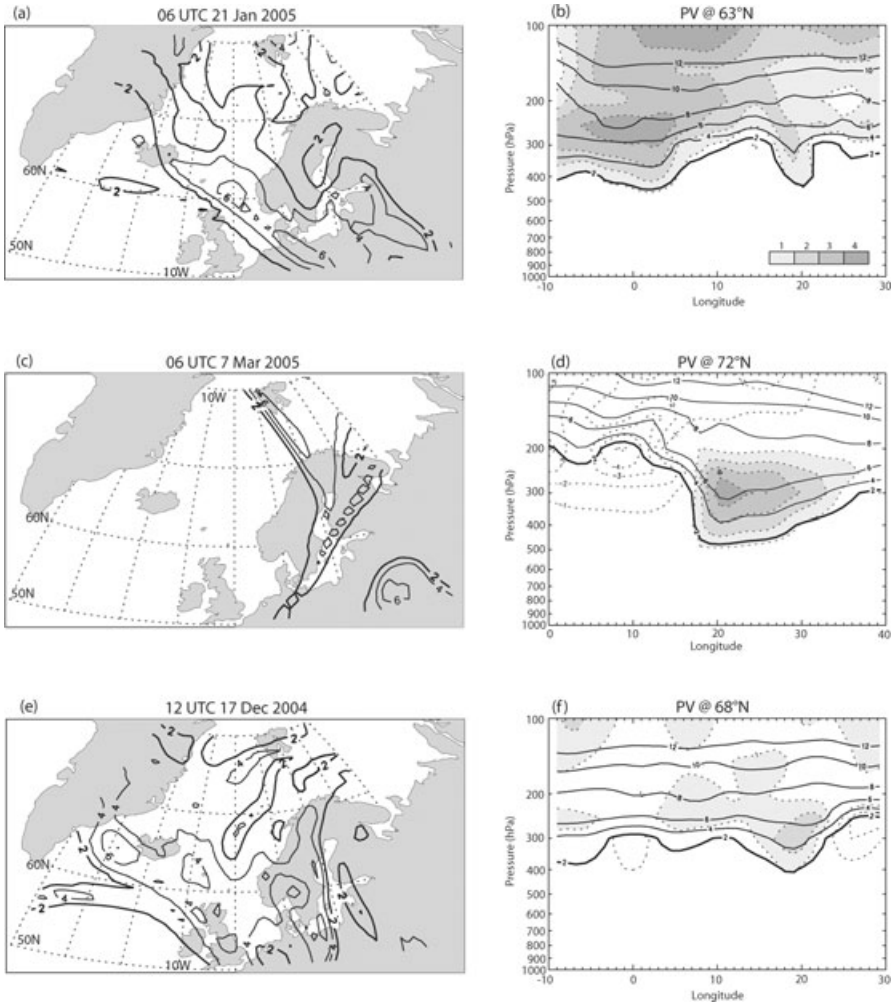


*Fig. 12.* Left-hand column: Potential Vorticity at 300 hPa (every 2 PV units). Right-hand column : cross-section of PV (solid contours) and PV anomaly relative to a monthly mean (dotted with positive anomaly shaded). (a) and (b), 21 January 2005 at 06 UTC, cross-section at 63°N; (c) and (d) 7 March 2005 at 06 UTC, cross-section at 72°N; (e) and (f) 17 December 2004 at 12 UTC, cross-section at 68°N. PV fields are from the operational ECMWF analyses.

characterize PL, since they are mesoscale and generally rather shallow phenomena. In addition, AMSU is made of two microwave modules (AMSU-A and B), with most channels insensitive to clouds, except those characterized by large ice particles. This property precisely makes possible the detection, even at the incipient stage and the tracking of PL. Moore and Von der Haar (2003) mainly considered AMSU-A channel 5 to identify the warm structure of a polar low, as well as complementary

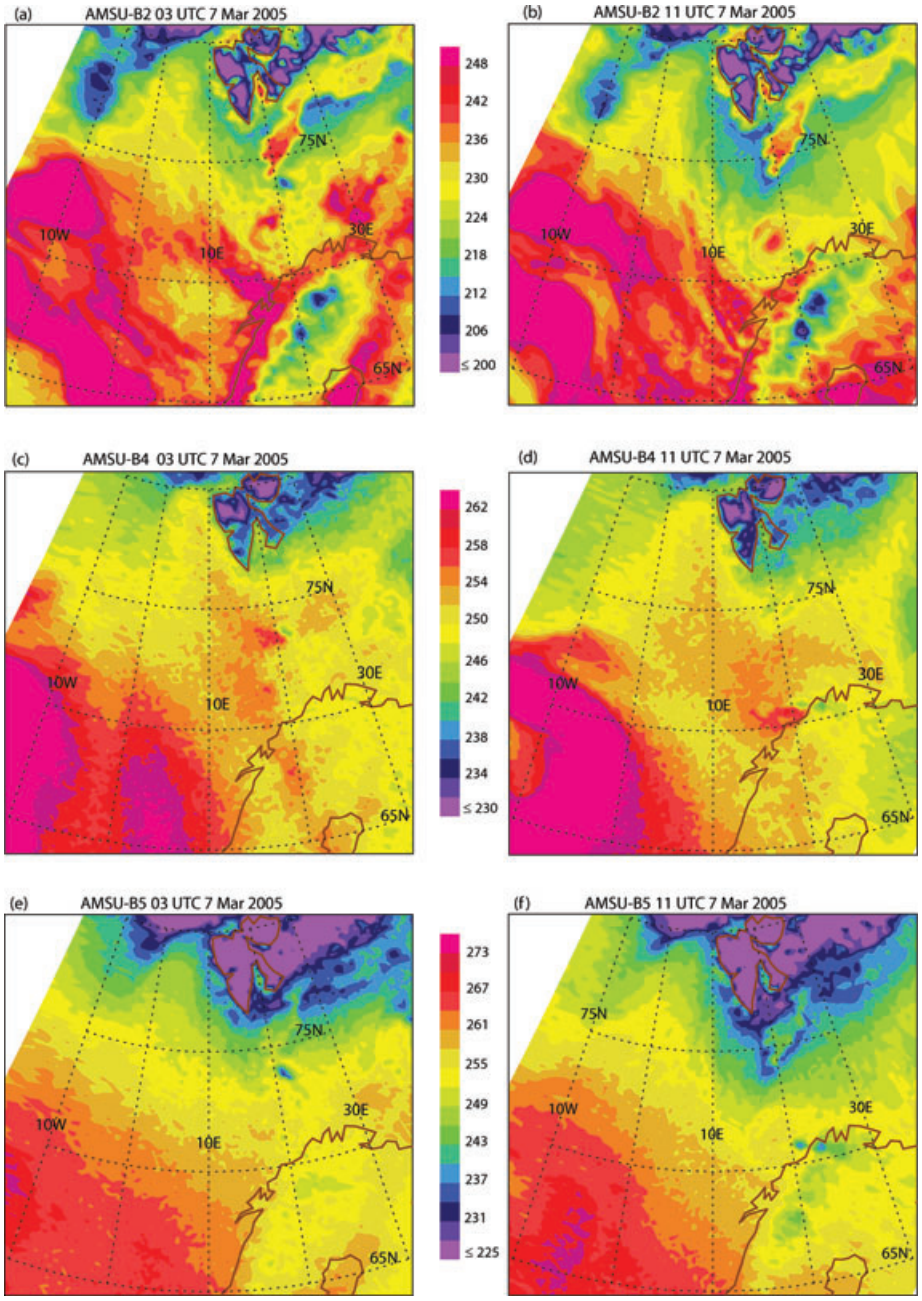


*Fig. 13.* AMSU-B channels 2, 4, 5 Brightness Temperature (in K) for 7 March 2005 at 03 (a, c, e) and 11 UTC (b, d, f). Observations at 03 UTC are from NOAA-16, whereas observations at 11 UTC are from NOAA-17.

information from AMSU-A3, B1 and B4 for cloud, surface and moisture effects that could possibly pollute the signal in the former. This study goes beyond these efforts, bringing the first attempt of using AMSU-B channels for an early detection and then tracking of the PL. In addition, the potential of AMSU-A to detect cold air outbreaks and upper-level structures that trigger polar low developments is also explored. We have focused on three case studies chosen to cover the spectrum of PL, that is, from mainly convective to mainly baroclinic.

We investigated the ability of the three channels that sound at 183 GHz and the channel at 150 GHz (AMSU-B channels 2–5) to track PL. A comparison with a radar image from Lofoten Island for a convective PL showed a good correspondence between depressed BT and the occurrence of precipitation. An early detection and tracking of convective PL is possible, in particular from AMSU-B4 and -B5. The AMSU-B2 has also some skill, but is less efficient when PL have a deep vertical extension, and also because it does not always show strong BT gradients

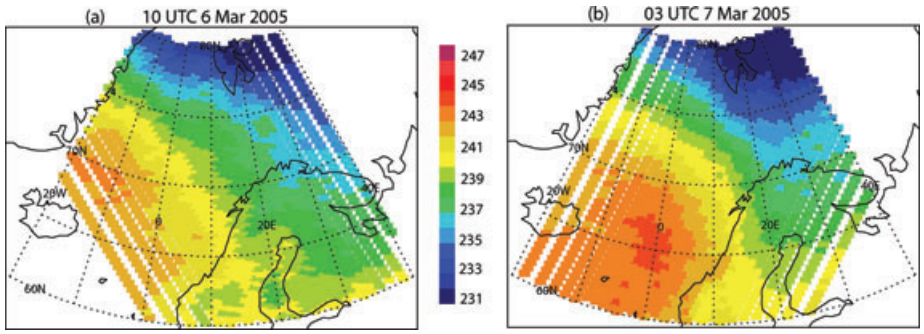


*Fig. 14.* Limb-corrected AMSU-A channel 5 Brightness Temperature (in K) for (a) 10 UTC 6 March and (b) 03 UTC 7 March 2005.

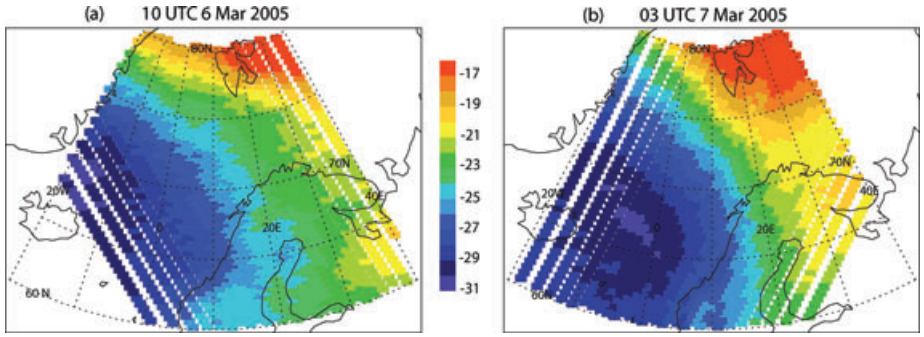


*Fig. 15.* Same as Figure 11 except for (a) 10 UTC 6 March and (b) 03 UTC 7 March 2005.

compared with the surroundings. However, for PL that are only weakly convective as it was the case for the PL on 7 March, the detection and the tracking from AMSU-B remains marginal.

The usefulness of AMSU-A channels for describing the synoptic environment in which PL develop has also been investigated. Channel 5, which peaks at about 5 km can clearly identify the cold air outbreaks associated with PL. However, a precise mesoscale description of the thermal structure of the systems, and in particular warm cores, is generally not possible, except very occasionnaly in the presence of a sufficiently large and deep signature.

Finally, among the different pre-conditioning conditions for PL developments, a PV trough is often encountered. Because of its stratospheric origin, the corresponding thermal signal of such intrusions is an increased temperature just around the tropopause. Using ECMWF PV fields for validating the coherent structures seen in AMSU-A data, we found that the difference between AMSU-A channels 7 and 5 channels was suitable for the detection of upper-level structures, as illustrated by the 21 January and 7 March 2005 cases. Conversely, for the 18 December 2004 case, the difference between channels 7 and 5 (not shown) did not exhibit marked structures, as it was also the case for ECMWF 300 hPa PV filelds (Figs. 12e and f). Clearly, this demonstrates the ability of AMSU to derive dynamic information in addition to thermal structures, allowing a better view of mesoscale weather systems in such data-sparse regions.

In spite of some limitations described in this study, our results have implications for PL forecasting. Information provided by AMSU-A channel 5 and by the difference between channels 7 and 5 can help to decide if a favourable environment for PL development has been set through the presence of cold air and instability in the troposphere. In operational forecasting of PL, the information on the state of the airmass, for example, instability, upper troughs and temperatures at 500 hPa, are almost all drawn from prognostic fields from numerical models. The method suggested here could provide an observational supplement to the prognosis and also be a useful tool in model verification (e.g. Chaboureau et al., 2000, 2008) in these areas, where other sources, such as for example actual soundings, are almost absent. In addition, the AMSU-B observations obviously add some information to the IR images currently used for forecasting purposes, since only cloud tops can be seen in the IR images, whereas AMSU-B has the potential to sound through the clouds. In particular, in the early phases of development, there is considerable uncertainty as to the nature of the various cloud structures. Often the initial disturbance is apparent just as a fuzzy stratus shield, with little clue as to what lies beneath. In those cases, an in depth view from the AMSU-B can be very useful, by showing the presence of convection. Besides, one of the main difficulties in the forecasting centres is to decide if a low is filling or deepening. The high temporal sampling that permits tracking of these structures at close time intervals, could help the diagnostic. An illustration of this point is provided by the model forecasts that

were produced for the 18 December 2004 case—cold air at 500 hPa (favourable for a PL development) but no close circulation at the surface (Figs. 4b and 6). AMSU-A channel 5 confirms the presence of a cold air outbreak (Fig. 8), and in addition, the detection of the incipient PL in the early hours of the day (Fig. 7) confirms the possibility of a PL reaching the Norwegian coast in the evening.

The results presented in this study are also relevant for climatological studies of polar low events. Such climatologies remain seldom and are, at the time being, of two types. The first type relies on extensive subjective IR-visible satellite imagery (Carleton, 1985; Forbes and Lottes, 1985; Harold et al., 1999). Caveats of such studies are their shortness (typically a couple of years), essentially because of the non-automatic character of the method and the uncertainty when attempting to strictly repeat such a technique. Alternatively, recent climatologies tend to define objective criteria to indentify PL from reanalyses (Condron et al., 2006; Bracegirdle and Gray, 2008). However, there are also limitations, which come from the representation of PL in such reanalyses (e.g. Condron et al., 2006 have shown that about 3 out of 4 for PL having a size between 100 and 500 km are not represented in ERA-40 data) and the rather low temporal frequency that precludes the tracking of PL. Investigation of microwave signature of PL may overcome some of these limitations because of the higher temporal resolution and the long period of time available. However, such climatology would be biased towards convective events since it would underestimate those possessing stronger low-level baroclinicity and weaker convection.

In a more general context about the use of microwaves, there have been discussions in the past to decide which microwave channels should be included in satellite missions that (also) aim at snowfall/high-latitude precipitation determination. For example, Bennartz and Bauer (2003), using 2-D and 3-D simulations of different precipitation events, showed the superiority of a channel at around 150 GHz over channels at 183 GHz. 150 GHz is optimal because it is at the same time highly sensitive to variations in ice scattering, and only moderately affected by variations in surface emissivity. Conversely, the water vapour sounding channels, which should be superior because of their little sensitivity to surface emission, have their scattering signal partially masked by the increased impact of water vapour in and above the clouds. They found that a $183 \pm 7$ GHz channel had an equally high sensitivity to ice particle scattering as the channel at 150 GHz only for very dry and low surface emissivity. As far as PL are concerned, this study shows the importance of channels at $183 \pm 3$ GHz (AMSU-B4) and $183 \pm 7$ GHz (AMSU-B5) and their advantages over the channel at 150 GHz (AMSU-B2).

Finally, although this study was intentionaly restricted to the use of AMSU data, it is clear that a more comprehensive picture of individual PL is given by the synergetic use of multiple satellite systems. Further studies should go into this direction.

## 6. Acknowledgments

AMSU data were obtained through the French Mixed Service Unit ICARE. We are grateful to B. Bruemmer for drawing our attention on the 7 March 2005 case.

## References

Bauer, P., Moreau, E., Chevallier, F. and O'Keefe, U. 2006. Multiple-scattering microwave radiative transfer for data assimilation applications. *Q. J. R. Meteorol. Soc.* **132**, 1259–1281.

Bennartz, R. and Bauer, P. 2003. Sensitivity of microwave radiances at 85–183 GHz to precipitating ice particles. *Radio Sci.* **38**, 8075, doi:10.1029/2002RS002626.

Bracegirdle, T. J. and Gray, S. L. 2008. An objective climatology of the dynamical forcing of polar lows in the Nordic Seas. *Int. J. Climatol.* **28**, 1903–1919, doi:10.1002/joc1686.

Brueske, K. F. and Velden, C. S. 2003. Satellite-based tropical cyclone intensity estimation using NOAA-KLM series Advanced Microwave Sounding Unit (AMSU) data. *Mon. Wea. Rev.* **131**, 687–697.

Buehler, S. A., Kuvatov, M. and John, V. O. 2005. Scan asymetries in AMSU-B data. *Geophys Res. Lett.* **32**, L248110, doi:10.1029/2005GL024747.

Carleton, A. M. 1985. On the interpretation and classification of mesoscale cyclones from satellite infrared imagery. *Int. J. Remote Sen.* **16**, 2457–2485.

Carleton, A. M., McMurdie, L. A., Katsaros, K. B., Zhao, H., Mognard, N.M. and co-authors. 1995. Satellite-derived features and associated atmospheric environments of Southern Ocean mesocyclone events. *Global Atmos.-Ocean Sys.*, **3**, 209–248.

Chaboureau, J.-P., Cammas, J.-P., Mascart, P., Pinty, J.-P., Claud, C. and co-authors. 2000. Evaluation of a cloud system life-cycle simulated by Meso-NH during FASTEX using METEOSAT radiances and TOVS-3I cloud retrievals. *Q. J. R. Meteorol. Soc.* **126**, 1735–1750

Chaboureau, J.-P., Söhne, N., Pinty, J.-P., Meirold-Mautner, I., Defer, E. and co-authors. 2008. A midlatitude precipitating cloud database validated with satellite observations. *J. App. Meteorol. Clim.* **47**, 1337–1353.

Claud, C., Katsaros, K. B., Petty, G. W., Chedin, A. and Scott, N. A. 1992a. A cold air outbreak over the Norwegian Sea observed with the TIROS-N Operational Vertical Sounder (TOVS) and the Special Sensor Microwave Imager (SSM/I). *Tellus* **44 A**, 100–118.

Claud, C., Scott, N. A. and Chedin, A. 1992b. Use of TOVS observations for the study of polar and arctic lows. *Int. J. Remote Sens.* **13**, 129–139.

Claud, C., Mognard, N. M., Katsaros, K. B., Chedin, A. and Scott, N. A. 1993. Satellite observations of a polar low over the Norwegian Sea by Special Sensor Microwave/Imager, Geosat and TIROS-N Operational Vertical Sounder. *J. Geophys. Res.*, **98**, 14 487–14 506.

Claud, C., Heinemann, G., Raustein, E. and McMurdie, L. 2004. Polar low le cygne: Satellite observations and numerical simulations. *Q. J. R. Meteorol. Soc.*, **130**, 1075–1102.

Claud, C., Duchiron, B. and Terray, P. 2007. Associations between large-scale atmospheric circulation and polar low developments over the North Atlantic during winter. *J. Geophys. Res.* **112**, D12101, doi:10.1029/2006JD008251.

Condron, A., Bigg, G. R. and Renfrew, I. 2006. Polar mesoscale cyclones in the northeast Atlantic : comparing climatologies from ERA-40 and satellite imagery. *Mon. Wea. Rev.* **134**, 1518–1533.

Demuth, J.L., Demaria, M., Knaff, J. A. and Vonder Haar, T. H. 2004. Evaluation of Advanced Microwave Sounding Unit tropical-cyclone intensity and size estimation algorithms. *J. Appl. Meteorol.* **43**, 282–296.

Duncan, C. N. 1977. A numerical investigation of polar lows. *Q. J. R. Meteorol. Soc.* **103**, 255–268.

Emanuel, K. A. 1986. An air-sea interaction theory for tropical cyclones, Part I: steady-state maintenance. *J. Atmos. Sci.* **43**, 585–604.

Emanuel, K. A. and Rotunno, R. 1989. Polar lows as arctic hurricanes. *Tellus* **41A**, 1–17.

Forbes, G. S. and Lottes, W. D. 1985. Classification of mesoscale vortices in polar airstreams and the influence of the large-scale environment on their evolution. *Tellus* **37A**, 132–155.

Funatsu, B. M., Claud, C. and Chaboureau, J. P. 2007. Potential of advanced microwave sounding unit to identify precipitating systems and associated upper-level features in the Mediterranean region : case studies. *J. Geophys. Res.* **112**, D17113, doi:10.1029/2006JD008297.

Gloersen, P., Mollo-Christensen, E. and Hubanks, P. 1989. Observations of Arctic Polar Lows with the NIMBUS-7 Scanning Multichannel Micowave Radiometer. In: *Polar and Arctic Lows* (eds P. F. Twitchell, E. A. Rasmussen and K. L. Davidson). A. Deepak Publishing, Hampton, VA, 359–371.

Goldberg, M. D., Crossby, D. S. and Whou, L. 2001. The limb-adjustement of AMSU-A observations: methodology and validation. *J. Appl. Meteorol.* **40**, 70–83.

Greenwald, T. J. and Christopher, S. A. 2002. Effect of cold clouds on satellite measurements near 183 GHz. *J. Geophys. Res.* **107**, 4170, doi:10.1029/2000JD000258.

Harold, J. M., Bigg, G. R. and Turner, J. 1999. Mesocyclone activity over the Northeast Atlantic, part 2: an investigation of causal mechanisms. *Int. J. Climatol.* **19**, 1283–1299.

Harrold, T. W. and Browning, K. A. 1969. The polar low as a baroclinic disturbance. *Q. J. R. Meteorol. Soc.* **95**, 710–723.

Heinemann, G. 1996. A wintertime polar low over the eastern Weddell Sea (Antarctica): a case study with AVHRR, TOVS, SSM/I and conventional data. *Meteorol. Atmos. Phys.* **58**, 83–102.

Heinemann, G. and Claud, C. 1997. Report of a Workshop on "Theoretical and Observational Studies of Polar Lows" of the European Geophysical Society Polar Lows Working Group. *Bull. Am. Meteorol. Soc.* **78**, 2643–2658.

Heinemann, G., Noel, S., Chedin, A., Scott, N. A. and Claud, C. 1995. Sensitivity studies of TOVS retrievals with 3I and ITPP retrieval algorithms: application to the resolution of mesoscale phenomena in the Antarctic. *Meteorol. Atmos. Phys.* **55**, 87–100.

Hewson, T. D., Craig, G. C. and Claud, C. 2000. Evolution and mesoscale structure of a polar low outbreak. *Q. J. R. Meteorol. Soc.* **126** (A), 1031–1063.

Kidder, S. Q., Goldberg, M. D., Zehr, R. M., Demaria, M., Purdom, J. F. W. and co-authors. 2000. Satellite analysis of tropical cyclones using the Advanced Microwave Sounding Unit (AMSU). *Bull. Am. Meteorol. Soc.* **81**, 1241–1259.

Lieder, M. and Heinemann, G. 1999. A summertime Antarctic mesocyclone over the Southern Pacific during FROST SOP 3: a meso-scale analysis using AVHRR, SSM/I, ERS and numerical model data. *Wea. Forecas.* **14**, 893–908.

Mansfield, D.A. 1974. Polar lows: the development of baroclnic disturbances in cold air outbreaks. *Q. J. R. Meteorol. Soc.* **100**, 541–554.

McMurdie, L. A., Claud, C. and Atakturk, S. 1997. Satellite-derived characteristics of Spiral and Comma-shaped southern hemisphere mesocyclones. *J. Geophys. Res.* **102**, 13 889–13 905.

Mo, T. 1999. AMSU-A antenna pattern corrections. *IEEE, Trans. Geosc. Remote Sens.* **37**, 103–112.

Moore, R. W. and Vonder Haar, T. H. 2003. Diagnosis of a polar low warm core utilizing the Advanced Microwave Sounding Unit. *Wea. Forecas.* **18**, 700–710.

Moore, G. W. K., Reader, M. C., York, J. and Sathyamoorthy, S. 1996. Polar Lows in the Labrador Sea: a case study. *Tellus* **48A**, 17–40.

Noer, G., and Ovhed, M. 2003. Forecasting of polar lows in the Norwegian and the Barents Sea, In: *Proceedings of the 9th Meeting of the European Polar Lows Working Group*,Cambridge, UK, 11–13 June 2003.

Nordeng, T. E. and Rasmussen, E. A. 1992. A most beautiful polar low. A case study of a polar low development in the Bear Island region. *Tellus* **44A**, 81–99.

Orlanski, I. 1975. A rational subdivision of scales of atmospheric processes. *Bull. Am. Meteorol. Soc.* **56**, 527–530.

Rasmussen, E. A. 1989. A comparative study of tropical cyclones and polar lows. In: *Polar and Arctic Lows* (eds P. F. Twitchell, E. A. Rasmussen and K. L. Davidson), A. Deepak Publishing, Hampton, VA, 47–80.

Rasmussen, E. A. and Turner, J. 2003. *Polar Lows : Mesoscale Weather Systems in the Polar Regions*, Cambridge University Press, Cambridge, 612 pp.

Rasmussen, E. A., Pedersen, T. S. Pedersen, L. T., and Turner, J. 1992. Polar lows and arctic instability lows in the Bear Island region. *Tellus* **44A**, 133–154.

Rasmussen, E. A., Turner, J. and Twitchell, P. F. 1993. Report of a workshop on applications of new forms of satellite data in polar low research. *Bull. Am. Meteorol. Soc.* **74**, 1057–1073.

Rasmussen, E. A., Claud C., and Purdom, J. F. 1996. Labrador Sea Polar Lows. *Global Atmos-Ocean Sys.* **4**, 275–333.

Saunders, R. W., Matricardi, M., Brunel, P., English, S., Bauer, P. and co-authors. 2005. RTTOV-8 Science and Validation Report. *Technical Report*. Numer. Wea. Predic. Satell. Appl. Facil., Exeter, UK, 41 pp.

Spencer, R. W. and Braswell, W. D. 2001. Atlantic tropical cyclone monitoring with AMSU-A: estimation of maximum sustained wind speeds. *Mon. Wea. Rev.*, **129**, 1519–1532.

Turner, J., Lachlan-Cope, T. A. and Moore, J. C. 1992. A comparison of satellite sounding data and aircraft measurements within a mature polar low. *Tellus*, **44A**, 119–132.

Turner, J., Lachlan-Cope, T. A. and Thomas, J. P. 1993. A comparison of Arctic and Antarctic mesoscale vortices. *J. Geophys. Res.* **98**, 13 019–13 034.

Wark, D. Q. 1993. Adjustement of TIROS Operational Vertical Sounder data to a vertical view. NOAA Tech. Report NESDIS-64, US Department of Commerce, Washington, DC, 36 pp.

Wilhelmsen, K. 1985. Climatological study of gale-producing polar lows near Norway. *Tellus* **37A**, 451–459.

Yao, Z., Lin, L., Chen, H. and Fei, J. 2008. A scheme for estimating tropical cyclone intensity using AMSU-A data. *Adv. Atmos. Sci.* **25**, 96–106.

Zhu, T., Zhang, D. L. and Weng, F. Z. 2002. Impact of the Advanced Microwave Sounding Unit measurements on hurricane prediction. *Mon. Wea. Rev.* **130**, 2416–2432.